PERFORMANCE OF A MAGNETICALLY SUSPENDED FLYWHEEL ENERGY STORAGE DEVICE

Markus Ahrens [1]
ICMB, ETH Zurich
Technopark PFA F16
8005 Zurich, Switzerland
email: ahrens@ifr.mavt.ethz.ch

Ladislav Kučera
ICMB, ETH Zurich
Technopark PFA F16
8005 Zurich, Switzerland
email: kucera@ifr.mavt.ethz.ch

René Larsonneur
MECOS Traxler AG
Gutstrasse 36
8400 Winterthur, Switzerland
email: larsonneur@ifr.mavt.ethz.ch

Abstract

This paper describes a high power flywheel energy storage device with 1 kWh of usable energy. A possible application is to level peaks in the power consumption of seam-welding machines.

A rigid body model is used for controller design, stability and robustness analysis.

Flywheel systems tend to have strong gyroscopic coupling which must be considered in the controller design. The gyroscopic coupling can cause instability in addition with system nonlinearities, digitization, time delay, filter characteristics and adaptive unbalance cancellation. Different approaches, such as decentralized control, controller design with LQR and cross feedback control are analyzed. Cross feedback control leads to a better system performance and is easy to implement.

Experimental results are given. The startup behaviour and the disturbing forces of the system while rotating are shown.

[1] corresponding author

1 Introduction

Latest developments in the field of composite materials and active magnetic bearings (AMB) have led to kinetic energy storage devices which are smaller and lighter and which operate at higher rotational speed. This increase of efficiency makes kinetic energy storage devices interesting for several fields of application.
Compared with kinetic energy storage devices static energy storage devices such as batteries or capacitors have limited lifetime cycles and low power and capacity.
Energy storage systems can be devided into two groups depending on their application. Long time energy storage with typical applications such as uninterruptible power supplies has long cycle times between loading and unloading energy. The main design goal here is to minimize losses during standby. Short time energy storage features many more load cycles per time unit, and the main design goal here is to minimize the losses during loading/unloading. In applications with extreme peaks in power consumption, such as seam-welding machines or island-type electrical networks, a short time energy storage device can level these peaks and, in addition, recover energy from the application.
For seam-welding machines there is a demand for an energy storage device with a capacity of 1 kWh of usable energy and high power (250 kW) of the motor/generator. This leads to a short time for loading/unloading of approximately 15 seconds.
For this reason a research project 'Kinetic Energy Storage (KIS)' was started at the ETH in 1992. The goal was to develop a kinetic short time energy storage system for stationary applications.

The system consists of the following key components.

- a composite fibre-reinforced high speed flywheel to store the energy
- active magnetic bearings to suspend the rotor
- a high speed motor/generator to provide power to and from the flywheel
- high efficiency power electronics for the motor/generator
- vacuum housing to reduce the friction losses

Magnetic bearings are ideally suited for high speed and vacuum applications due to their contact free operation, low friction losses, adjustable damping and stiffness characteristics

and due to the fact that no lubricants are necessary.

A magnetic bearing system is unstable in nature and, therefore, a controller is required. For a controller design a mathematical model of the plant is necessary.

The rotor can be described as a $\boldsymbol{MDGK}$-system (see equation 1). The gyroscopic matrix $\boldsymbol{G}$ describes the coupling between the rotor axes while rotating.

For rotors with a small ratio of the moments of inertia ($J_z/J_x \ll 1$, see figure 1) the influence of $\boldsymbol{G}$ respectively of the rotational speed is small and can be neglected. In this case the system can be devided into two identical subsystems (x-z- and y-z-plane), which can be controlled independently. Furthermore, for many weakly gyroscopic magnetic bearing applications decentralized controllers can be used [Ble84].

However, if the gyroscopic effects become strong ($J_z/J_x \not\ll 1$) stability problems may occur. While conservative systems remain stable even under gyroscopic effects [MS76], magnetically suspended rotors can be destabilized with increasing rotational speed, thus, they can no longer be considered conservative. There are mainly two reasons why stability cannot be guaranteed for such magnetic bearing systems. In [Her91] it is pointed out that the plant is not positive-real when digital controllers are used or when sensor-actuator collocation cannot be fulfilled. In [ME93] it is shown that gyroscopic effects can also cause instability when certain nonlinearities are considered.

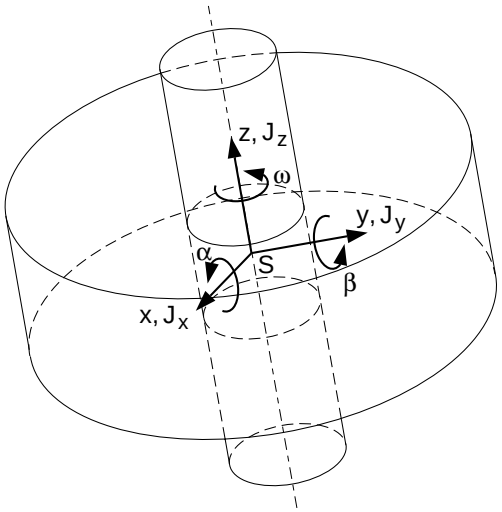

Figure 1: Definition of the coordinate system and of the moments of inertia

S: centre of gravity, ω: rotational speed, J_x: moment of inertia around x-axis (y, z analogous)

For rotors with a ratio of the moments of inertia which is not small ($J_z/J_x \not\ll 1$) (e.g. pumps, turbines and especially flywheels) or for rotors with extremely high rotational speed the influence of gyroscopic effects must be considered in order to avoid instability and to achieve better system performance ([MH84], [ONS89], [AK95]).

2 Description of the Flywheel Energy Storage System

The system features an inner type stator with the radial magnetic bearings (see figures 2, 3, 4). The composite flywheel is connected to the outer type rotor with a cone interference fit. The rotor itself consists of an inner and an outer part, with the stator of the electrical machine in between (see figure 3). One single thrust bearing on the top of the rotor carries the weight.

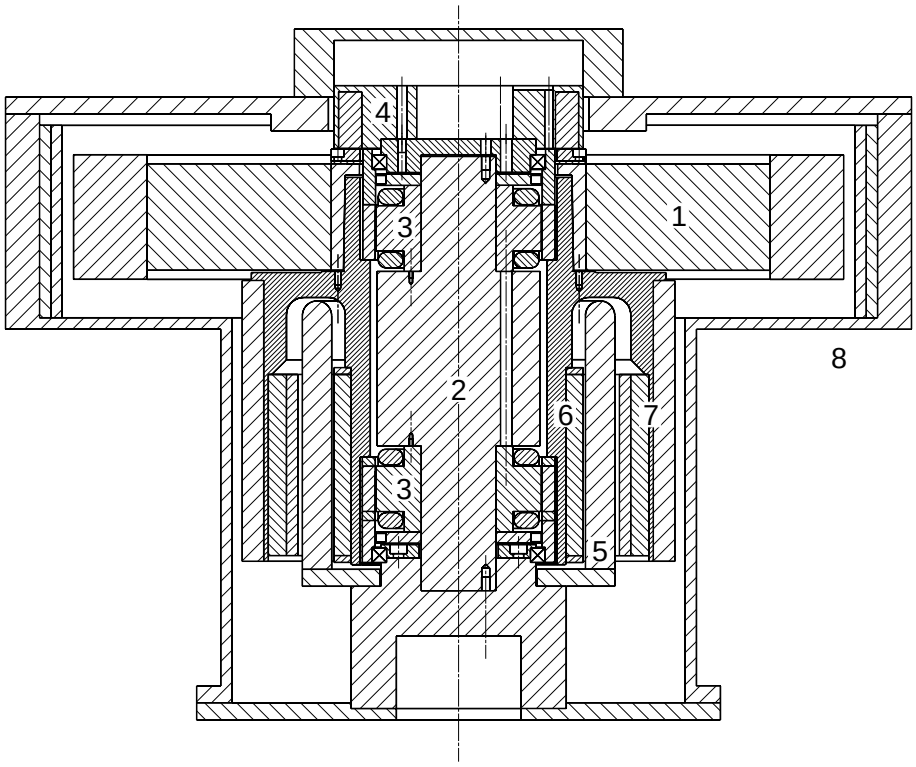

Figure 2: Cross section of the flywheel energy storage system

1: flywheel, 2: stator of the radial magnetic bearings with water cooling, 3: radial magnetic bearings, 4: thrust magnetic bearing, 5: stator of the electrical machine with water cooling, 6: inner rotor part, 7: outer rotor part, 8: vacuum housing

Table 1: Data of the KIS system

diameter of the housing	: 870 mm
height of the housing	: 810 mm
diameter of the flywheel	: 680 mm
length of the rotor	: 365 mm
total mass of the rotor	: 175 kg
nominal speed	: 15000 rpm
no-load speed	: 7500 rpm
usable energy	: 1 kWh
nominal power	: 250 kW
diameter of radial AMBs	: 148 mm
nominal air gap	: 0.6 mm
air gap of the retainer bearings	: 0.3 mm
maximum (static) thrust AMB force	: 2000 N
maximum (static) radial AMB force	: 400 N
sampling frequency of the AMB controller	: 4 kHz

The highest circumferential velocity of the flywheel is about 600 m/s. In case of failure the energy stored in the flywheel can cause considerable damage to the whole system. Therefore, the flywheel for this project was wound with orthotropic composite materials (woven bands of glass and carbon fibre). This leads to a good failure behaviour [vB95].

Due to the small power dissipation in vacuum the electrical machine was optimized to reduce the eddy current losses in the rotating part during loading/unloading and standby. Therefore, a synchronous motor (3 pole pairs, 3 phases) with lamination sheets on the inner rotor and permanent magnets mounted on lamination sheets on the outer rotor is used.

For the KIS system two 3-point inverted rectifiers are used. They have a low fundamental frequency but come up with a well-shaped sinusoidal waveform for voltage and current. This leads to a high efficiency of the power electronics [SG93].

The rotor is suspended by one thrust and two radial current-controlled active magnetic bearings. The thrust bearing carries the weight of the rotor (static force). The disturbing forces for the thrust bearing are small. The radial bearings are inside of the rotor. They do

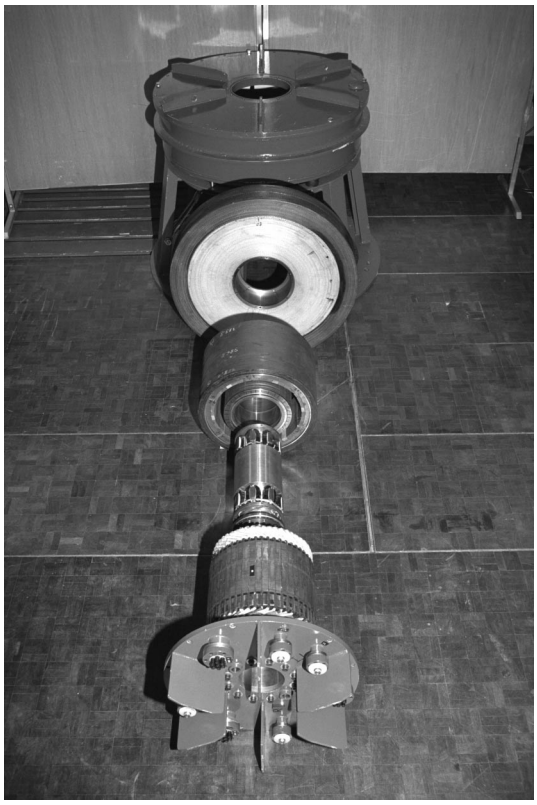

Figure 3: The kinetic energy storage system KIS
From above: housing, flywheel, rotor, stator of the radial magnetic bearings, stator of the electrical machine

not have to carry static forces, however, radial disturbing forces, mainly due to unbalance, occur. A special adaptive feedforward unbalance cancellation algorithm is implemented to cancel out these undesired periodic disturbances (see section 3.6).

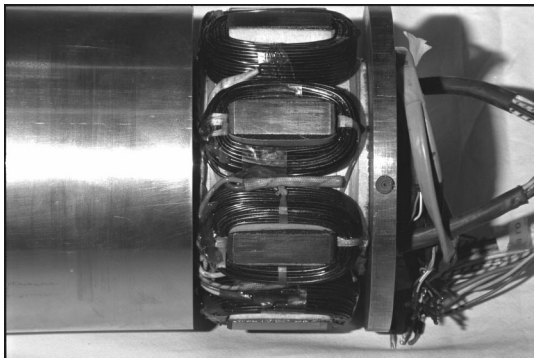

Figure 4: A radial bearing and a carrier ring with the radial sensors

3 Control of Gyroscopic Systems

3.1 Rotordynamic Model

The equations of motion for the magnetically levitated rotor can be written as

$$\bar{\boldsymbol{M}}\ddot{\boldsymbol{q}} + (\bar{\boldsymbol{D}} + \omega\bar{\boldsymbol{G}})\dot{\boldsymbol{q}} + \bar{\boldsymbol{K}}\boldsymbol{q} = \bar{\boldsymbol{F}} \tag{1}$$

In equation 1 $\boldsymbol{q}$ is the displacement vector, $\bar{\boldsymbol{M}}$ the symmetric positive definite mass matrix, $\bar{\boldsymbol{D}}$ the symmetric positive semi-definite inner damping matrix, $\bar{\boldsymbol{G}}$ the skew-symmetric gyroscopic matrix, $\bar{\boldsymbol{K}}$ the symmetric positive semi-definite stiffness matrix and $\bar{\boldsymbol{F}}$ the vector of the external forces (including the magnetic bearing forces).

A modal analysis has shown that the rotor can be regarded as rigid. The first rotor flexural mode is 484 Hz. The maximum rotational speed is 250 Hz and therefore a rigid body model is used for controller design. No spillover problems were experienced with flexural modes.

Equations 2 to 5 describe the rotor motion split up into the two subsystems (x-z- and y-z-plane).

$$\begin{bmatrix} \boldsymbol{M} & \boldsymbol{0} \\ \boldsymbol{0} & \boldsymbol{M} \end{bmatrix} \begin{bmatrix} \ddot{\boldsymbol{q}}_1 \\ \ddot{\boldsymbol{q}}_2 \end{bmatrix} + \left[\begin{bmatrix} \boldsymbol{D} & \boldsymbol{0} \\ \boldsymbol{0} & \boldsymbol{D} \end{bmatrix} + \omega \begin{bmatrix} \boldsymbol{0} & \boldsymbol{G} \\ -\boldsymbol{G} & \boldsymbol{0} \end{bmatrix} \right] \begin{bmatrix} \dot{\boldsymbol{q}}_1 \\ \dot{\boldsymbol{q}}_2 \end{bmatrix} + \begin{bmatrix} \boldsymbol{K} & \boldsymbol{0} \\ \boldsymbol{0} & \boldsymbol{K} \end{bmatrix} \begin{bmatrix} \boldsymbol{q}_1 \\ \boldsymbol{q}_2 \end{bmatrix} = \begin{bmatrix} \boldsymbol{F}_1 \\ \boldsymbol{F}_2 \end{bmatrix} \tag{2}$$

$$\begin{bmatrix} \boldsymbol{y}_1 \\ \boldsymbol{y}_2 \end{bmatrix} = \begin{bmatrix} \boldsymbol{C} & \boldsymbol{0} \\ \boldsymbol{0} & \boldsymbol{C} \end{bmatrix} \begin{bmatrix} \boldsymbol{q}_1 \\ \boldsymbol{q}_2 \end{bmatrix} \tag{3}$$

Here, $\boldsymbol{C}$ is the output matrix, $\boldsymbol{y}$ the output vector, index 1 represents the x-direction and index 2 the y-direction. The gyroscopic cross coupling, which depends on the rotational speed and couples the motion in x- and in y-direction, can be seen in equation 2.

For a rigid body model the displacement vectors $\boldsymbol{q_1}$ and $\boldsymbol{q_2}$ are as follows (see figure 1).

$$\boldsymbol{q_1} = \begin{bmatrix} \beta \\ x \end{bmatrix} \tag{4}$$

$$\boldsymbol{q_2} = \begin{bmatrix} -\alpha \\ y \end{bmatrix} \tag{5}$$

3.2 Behaviour of a Magnetically Suspended Gyroscope

In this section the basic behaviour of gyroscopes with magnetic suspension is shown. More information on the behaviour of gyroscopes in general can be found in [Mag71].

For simplicity the system behaviour is shown for a linearized bearing model using decentralized PD-control. In this case the rotor behaves like an elastically suspended gyroscope (suspension with spring and damper).
Its motion can be described by equation 2 using the matrices $\boldsymbol{M} = \boldsymbol{M}^{\boldsymbol{T}} > 0, \boldsymbol{K} = \boldsymbol{K}^{\boldsymbol{T}} \geq 0, \boldsymbol{D} = \boldsymbol{D}^{\boldsymbol{T}} \geq 0$. Such a system cannot be destabilized by gyroscopic effects [MS76].

The non-rotating system has two pairs of two rigid body eigenfrequencies which are equal for the x-z- and the y-z-plane. With increasing rotational speed these eigenfrequencies change as a consequence of the gyroscopic coupling. The four eigenfrequencies are the nutation ω_N, two pendulous ω_{pe} and the precession frequency ω_P. The nutation frequency increases with the rotational speed ($\lim_{\omega\to\infty} \omega_N = \omega\frac{I_z}{I_x}$), while the precession frequency decreases ($\lim_{\omega\to\infty} \omega_P = 0$). The two pendulous eigenfrequencies converge to constant values. Figure 5 shows the gyroscopic dependence of the rotor eigenvalues in the complex plane. Figure 6 shows the same dependence for the eigenfrequencies in a Campbell diagram.

For the KIS system it can be seen that the nutation frequency increases strongly and that the precession mode becomes limit stable at high rotational speed. The eigenfrequencies at standstill are in the range of 15 to 20 Hz. With a decentralized PD-controller the precession frequency would be nearly 0 Hz and the nutation frequency 300 Hz at end rotational speed (250 Hz). Although a gyroscopic system with PD-control is stable in theory the gyroscopic coupling leads to instability problems in practice (see section 3.5). Fixed gain centralized control designed with LQR usually cannot avoid instability (see section 3.3) unless special design techniques are applied to increase system robustness. For the KIS system cross feedback control which considers the gyroscopic coupling leads to a better system performance and avoids instability (see section 3.4).

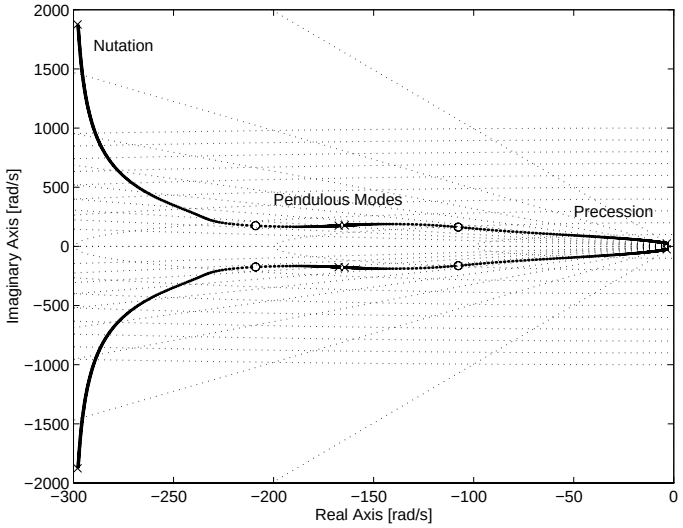

Figure 5: Poles of the closed-loop system depending on the rotational speed (decentralized PD-control), rotational speed $\omega = 0 \ \ldots \ 1600\,\mathrm{rad/s}$

$\circ$: poles at $\omega = 0\,\mathrm{rad/s}$

$\times$: poles at $\omega = 1600\,\mathrm{rad/s}$

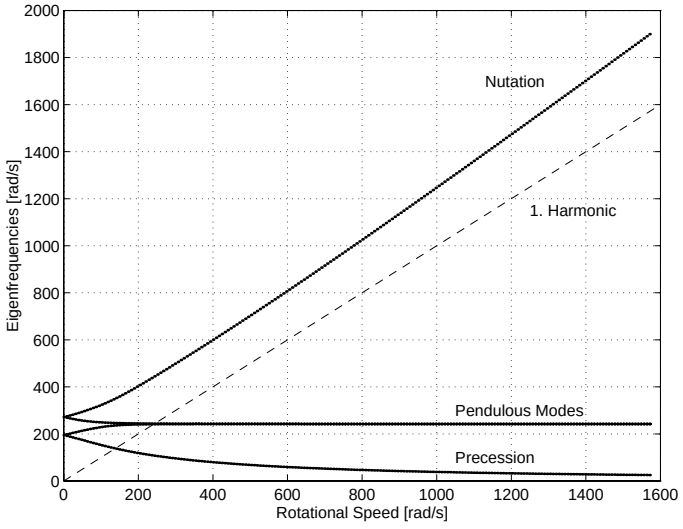

Figure 6: Campbell diagram for the rigid body model, $\omega = 0 \ldots 1600\,\mathrm{rad/s}$ (decentralized PD-control)

3.3 Controller design with LQR

Controller design with LQR minimizes the cost function J and, therefore, the actuator energy. $\boldsymbol{x}$ is the state vector and $\boldsymbol{u}$ is the control input vector.

$$J = \int_0^\infty (\boldsymbol{x'Qx} + \boldsymbol{u'Ru})\mathrm{d}t \tag{6}$$

Feedback law

$$\boldsymbol{u} = -\boldsymbol{K}\boldsymbol{x} \tag{7}$$

Usually the weighting matrices $\boldsymbol{Q}$ and $\boldsymbol{R}$ can be chosen as identity matrices. For magnetic bearing systems controller design with LQR normally leads to a system with too low stiffness and too much relative damping. Therefore, $\tilde{\boldsymbol{Q}} = \beta\boldsymbol{Q},\ \beta > 1$ must be chosen, which increases the stiffness of the system.

As a result of the LQR design feedback gain matrix $\boldsymbol{K}$ is full, thus the controller is fully centralized. Compared with a decentralized controller the computational time is much longer when digital control is applied.

LQR centralized control has better system performance if only the design rotational speed is considered. However, instability of the closed-loop system may occur when the rotational speed changes. This effect is related to the non-conservative forces introduced by the fully coupled controller (see figure 7 or [Ulb79]). In order to avoid this instability a controller designed with LQR has to depend on the rotational speed by using look-up tables. Figure 8 shows that even then the stability margin for the nutation and the precession mode decreases with increasing rotational speed.

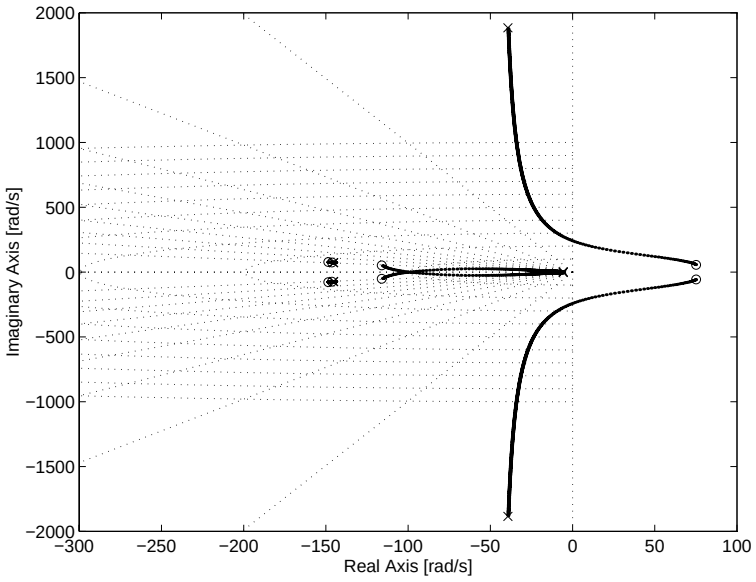

Figure 7: Poles of the closed-loop system, controller design at $\omega = 800\,\mathrm{rad/s}$, (LQR-controller design), rotational speed $\omega = 0 \ldots 1600\,\mathrm{rad/s},\ \beta = 8$

$\circ$: poles at $0\,\mathrm{rad/s}$

$\times$: poles at $1600\,\mathrm{rad/s}$

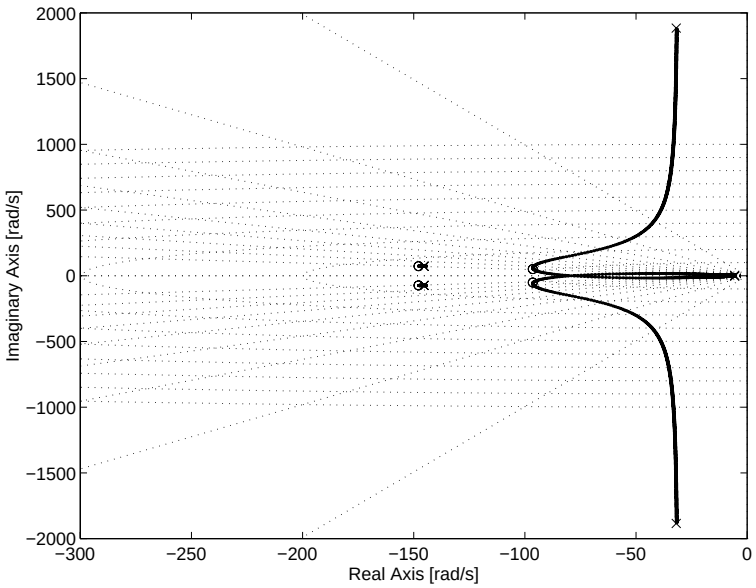

Figure 8: Poles of the closed-loop system, (LQR-controller design for varying rotational speed), design rotational speed $\omega_{des} = 0 \ldots 1600\,\mathrm{rad/s},\ \beta = 8$

$\circ$: poles at $0\,\mathrm{rad/s}$

$\times$: poles at $1600\,\mathrm{rad/s}$

3.4 Cross Feedback Control

In the previous sections it was shown that decentralized PD-control as well as fully centralized control with LQR design significantly loose stability margin or cannot avoid instability due to gyroscopic effects. Hence, more suitable control design techniques must be considered.

It might be possible to account for the gyroscopic coupling with modern robust control design techniques. However, a straight forward approach is taken here because the destabilizing gyroscopic effects are exactly known and therefore a physical interpretation is possible.

In the following cross feedback control which compensates for gyroscopic effects is analyzed. Figure 9 shows a simple realization of a decentralized controller augmented by an additional feedback path for the compensation of the gyroscopic cross coupling. This controller expansion is small and, therefore, computational time will not increase much. Compared to a fully centralized feedback matrix the computational time is nearly four times shorter. Furthermore, the implementation of this compensation is simple and control parameters can be found based on physical interpretation.

A complete compensation of the gyroscopic effects is possible in theory, but leads to instability in practice mainly due to time delay. An attenuation factor C_{att} is used to improve robustness. The structure of the compensator remains the same. The attenuation factor gives the ratio of the implemented compensation compared to a complete compensation.

The cross feedback term k_c (see figure 9) is

$$k_c = C_{att} \frac{\omega J_z}{k_i L_{mb}^2} \tag{8}$$

Here, L_{mb} is the distance between the two radial bearing planes and k_i is the force-current factor of a radial bearing.

A sufficient and robust solution can be found with an attenuation factor of 75%. With complete compensation the system has the same behaviour as at standstill even at nominal rotational speed. With reduced compensation (e.g. 75%) the system behaviour is the same as for a reduced rotational speed (25% of the nominal rotational speed).

Figure 10 shows that the influence of the gyroscopic coupling can be significantly reduced with cross feedback control compared with decentralized PD-control (figure 5) or speed dependent LQR-control (figure 8). Figure 11 shows measured frequency response functions

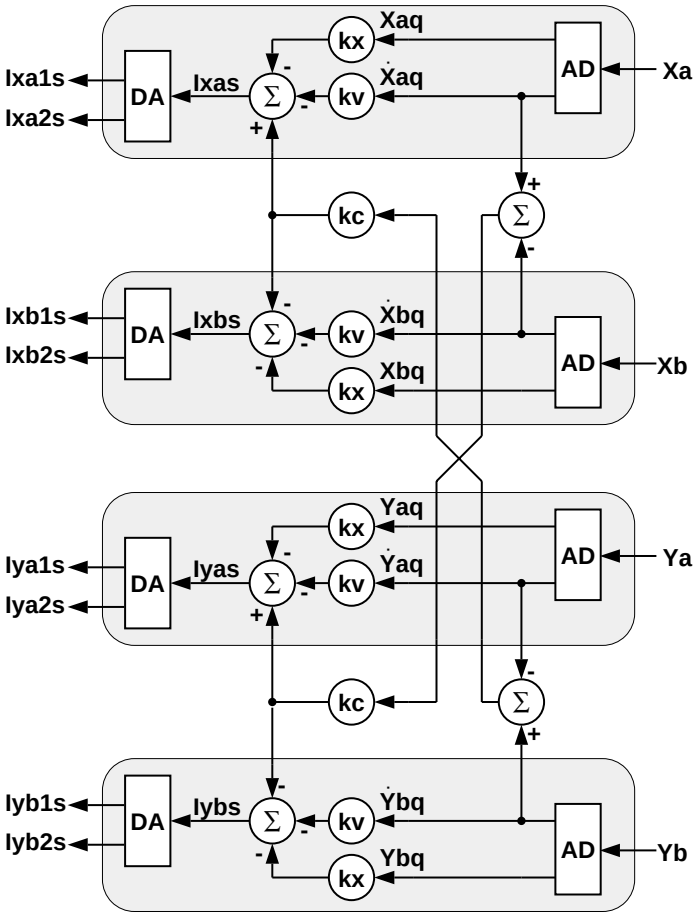

Figure 9: Decentralized controller with compensation of the gyroscopic cross coupling

using decentralized control with cross feedback. As can be seen the nutation and precession mode can be influenced as expected. The measured eigenfrequencies correspond perfectly with calculated results. It can be seen that with increasing attenuation factor the precession frequency increases and the nutation frequency decreases. Furthermore, the damping of both modes increases significantly.

Figure 12 shows measurements of the rotor motion with and without cross feedback control. It can be seen that the precession mode becomes limit stable using only decentralized control (left plot). With additional cross feedback control the precession frequency and the damping of the precession mode both increase as expected from the eigenvalue computation (figure 10). This important increase in system performance is clearly documented in figure 12 (right plot).

Additional nonlinear analysis shows that the stability margin is further decreased by elements

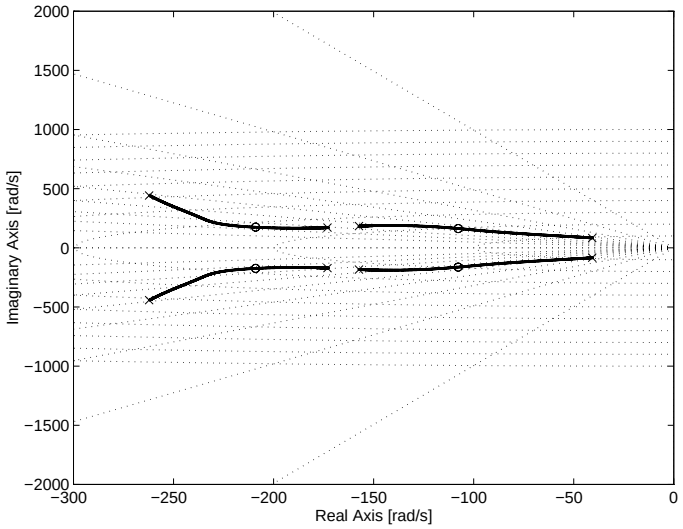

Figure 10: Poles of the closed-loop system depending on the rotational speed, cross feedback control ($C_{att} = 0.75$), rotational speed $\omega = 0 \ldots 1600\,\mathrm{rad/s}$
$\circ$: poles at $\omega = 0\,\mathrm{rad/s}$
$\times$: poles at $\omega = 1600\,\mathrm{rad/s}$

with a phase shift, e.g. digitization or time delay [AK95]. Hence, by implementing the proposed compensation scheme, instability cannot be avoided but occurs at much higher rotational speed than with LQR-control or simple PD-control with necessary filtering.

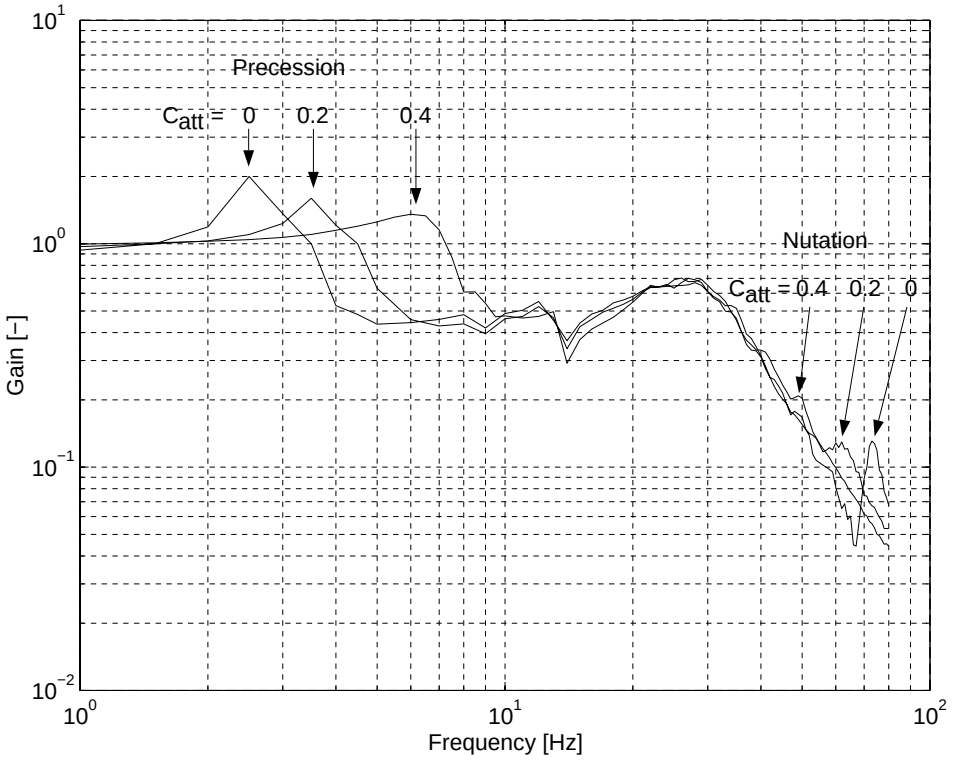

Figure 11: Measured closed-loop transfer function of the plant and the controller for decentralized control ($C_{att} = 0$) and cross feedback control ($C_{att} = 0.2$ and 0.4), rotational speed $\omega = 50\,\mathrm{Hz}$

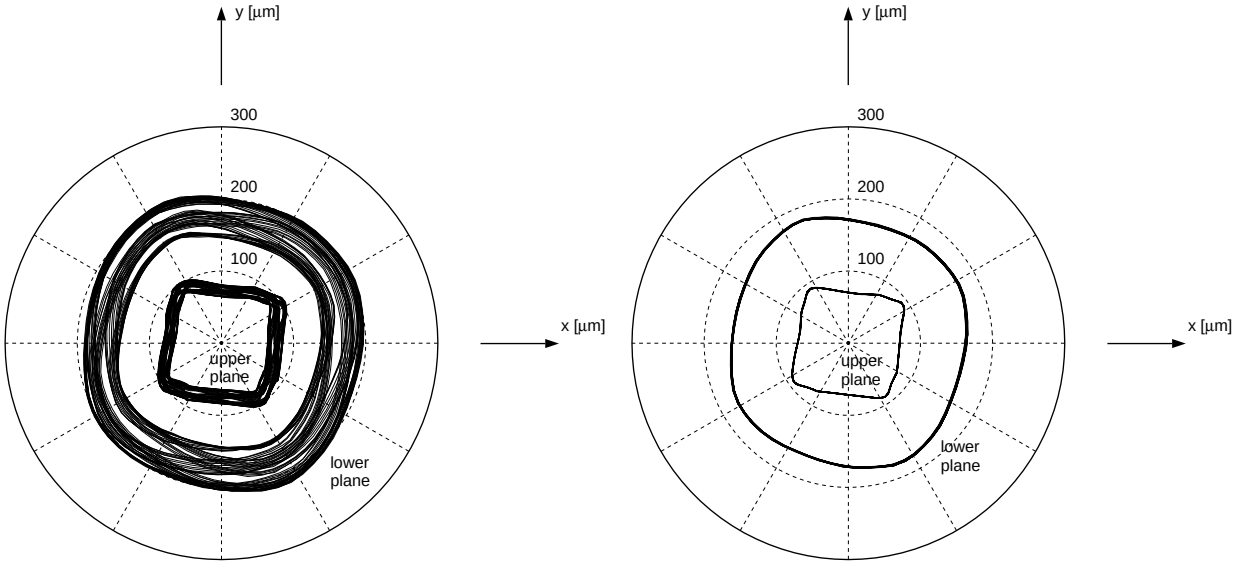

Figure 12: Measured x-y-plot of the rotor motion in the two radial bearing planes, rotational speed 4000 rpm

left plot: decentralized control, right plot: cross feedback control ($C_{att} = 0.1$)

3.5 Filtering and Integrating Feedback

For practical applications an integrator part within the control scheme is necessary to avoid a steady-state position error. Furthermore, a low pass filter included in the controller is necessary in order to reduce the feedback gain for higher frequencies (noise, resonances of the housing, dynamic amplifier saturation). Figure 13 shows a Bode plot of a decentralized controller with integrator and filter. The system has two frequency ranges where the open-loop phase is $< -180°$. Thus, instability can occur when the open-loop gain is larger than 1 which may happen for system resonances. As mentioned before the eigenfrequencies of a gyroscopic system depend on the rotational speed (nutation, precession). Therefore, the integrator part can cause instability for the precession mode and the low-pass filter will tend to destabilize the nutation mode.

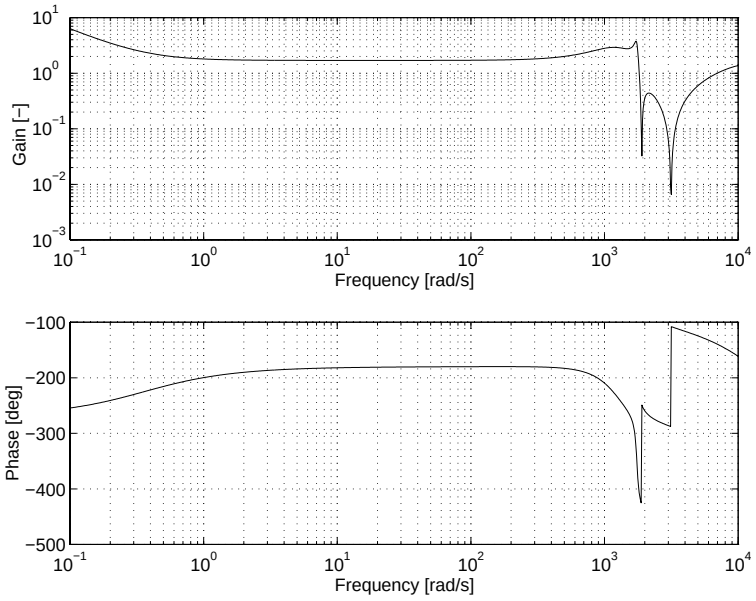

Figure 13: Bode plot of a decentralized discrete-time PID-controller with integrating feedback and 4th order low pass elliptical filter (cut-off frequency 1760 rad/s)

An analysis of the system behaviour with cross feedback control, low pass filter and integrating feedback shows that all closed-loop poles including filter poles depend on the rotational speed. Instability cannot be avoided if the filter and integrator characteristics are not properly chosen. Therefore, the choice of a suitable filter type with appropriate filter parameters is crucial. Another possibility to avoid instability is to use different filters for the cross feedback path and for the decentralized controller. For a system with a pure cross feedback path

without filter instability does not occur. For practical applications, however, filtering for the cross feedback path will be necessary as well.

3.6 Adaptive Unbalance Compensation

One of the most common sources of undesired rotor vibration are the displacements and forces generated by residual rotor unbalances. Differing from conventional bearings active magnetic bearings can overcome this problem quite easily by inserting an adaptive feedforward unbalance compensation scheme into the feedback loop.

A generalized theory of unbalance compensation using magnetic bearings is presented in a different location within this volume [HBGL96]. Here, only the stability problems of such adaptation schemes associated with the strong gyroscopic effects of the given flywheel are briefly discussed.

As can be seen in [HBGL96], [LH94] the overall system stability with adaptive unbalance compensation is determined from the system's sensitivity matrix $\boldsymbol{S}$ evaluated at rotational speed ω:

$$\mathrm{eig}(\boldsymbol{T}\boldsymbol{S}(j\omega)) = -\lambda_k,\ k = 1, \ldots, 4 \tag{9}$$

The complex matrix $\boldsymbol{T}$ in equation 9 comprises the parameters of the adaptation process and determines system stability. The values of λ_k correspond to the angles of departure of the root locus when the adaptation loop is closed, thus are given desired numbers. Overall closed-loop stability is achieved if all eigenvalues λ_k have negative real parts. The adaptation speed is given by the magnitude of λ_k. The sensitivity matrix $\boldsymbol{S}$ can be obtained easily by using the magnetic bearing itself as an actuator and by performing an FFT on the measured input and output signals of $\boldsymbol{S}$.

For weakly gyroscopic systems the problem to determine parameter matrix $\boldsymbol{T}$ is trivial: since the off-diagonal terms of $\boldsymbol{S}$ are small a diagonal choice of $\boldsymbol{T}$ will directly yield a feasible solution. For a strongly gyroscopic system, however, $\boldsymbol{S}$ will be a dense matrix, and a solution for equation 9 is much more cumbersome to find. Possible approaches are:

A. $\boldsymbol{T} = \boldsymbol{S}^{-1}(j\omega)$

B. Exact solution for $\boldsymbol{T}$ by numerically solving a system of polynomials in the complex unknown elements of $\boldsymbol{T}$

C. Reduction of the gyroscopic influence in $\boldsymbol{S}$ by implementing cross feedback control (see section 3.4)

Case A yields an angle of π of the root locus and, thus, optimum stability conditions. However, the inverse of $\boldsymbol{S}$ must be determined for a number of different rotational speeds and stored in a look-up table. The number of real-time computations for this approach is quite large.

Case B is mathematically rather complex and can only be solved numerically, e.g. by applying homotopic continuation methods. Furthermore, the whole process must be carried out for several rotational speeds ω, since the sensitivity matrix $\boldsymbol{S}$ will change with increasing speed.

In this project approach C seems to be most promising since cross feedback must anyhow be implemented for the main magnetic bearing controller in order to drastically reduce gyroscopic influence (see section 3.4). As a consequence $\boldsymbol{S}$ will result in a quasi-diagonal matrix with only small off-diagonal terms. Furthermore, $\boldsymbol{S}$ will change much less with rotational speed so that the need for a look-up table vanishes. Due to the quasi-diagonal structure of $\boldsymbol{S}$ the parameter matrix $\boldsymbol{T}$ for the unbalance adaptation process can then be chosen diagonal and the solution for equation 9 will again be trivial (see above).

4 System Behaviour

4.1 Startup and Standstill Operation

Due to the motor design there is only space for one thrust bearing on the top of the rotor. This leads to nonlinear bearing and sensor characteristics with different behaviour in upwards and downwards directions. When the rotor is in the lower retainer bearing the axial air gap is at its maximum. Here, a magnetic force of about 2000 N is necessary to lift up the rotor. When levitating the axial air gap is smaller and, therefore, the maximum magnetic force capacity is much higher. A controller which can lift up the rotor has a gain which is too high at the operating point. Therefore, two controller sets are used. The first operates for large axial air gaps and has a large gain. This one is used for the startup. The second one is used in normal operation and operates for small axial air gaps. The switch of the controller sets depends on the axial displacement.

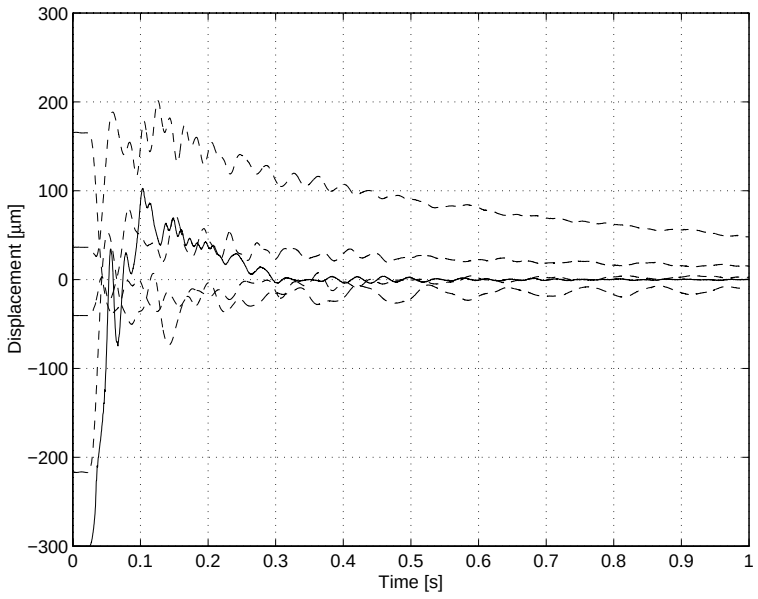

Figure 14: Startup of the rotor
solid line: axial displacement
dashed lines: radial displacements

Figure 14 shows the startup of rotor. Plotted are the axial and the four radial position signals. It can be seen that the integrator part of the radial controllers is chosen to be small

in order to avoid instability of the precession mode when rotational speed increases. While levitating the noise level is about 6 bits (less than 1 μm).

4.2 Behaviour at Rotation

Figure 15 shows the measured open-loop transfer function of the plant (rotor including sensor filter and actuator dynamics) for the upper and lower radial bearing. The system resonances in the frequency range between 100 and 400 Hz arise from the overall mechanical setup (housing). Since nutation mode will pass through this frequency range the problem of large resonance amplitudes might occur. Presently, the origin of the resonances is investigated and measures will be taken to eliminate the undesired housing eigenmodes.

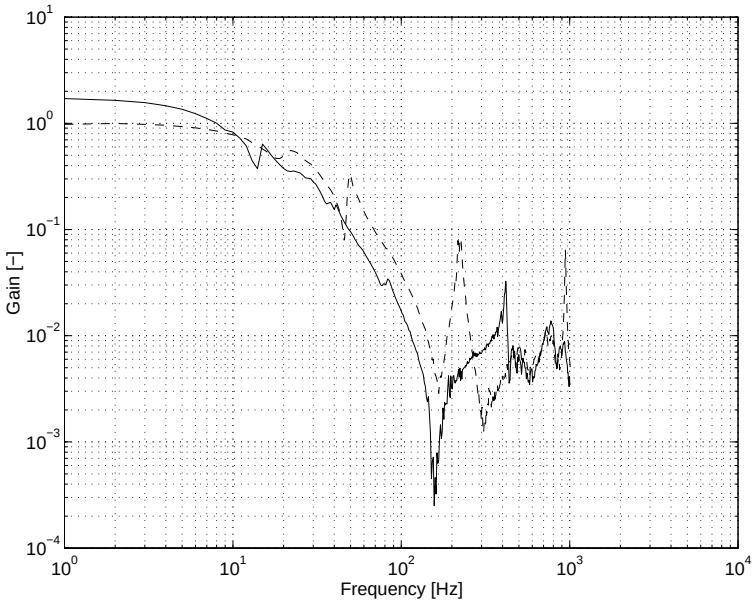

Figure 15: Measured transfer function of the plant
solid line: upper radial bearing
dashed line: lower radial bearing

Normally unbalance is the most important disturbance force for rotor systems. However, by using the unbalance cancellation method described in section 3.6 these disturbances can be overcome. Due to the high power of the electrical machine other harmonic disturbance forces are existing. A FFT of the radial position signals (figure 16) shows that the first (unbalance) and third (number of pole pairs of the motor) harmonic signal components are dominant.

The corresponding motion of the rotor, caused by the disturbing force, is shown in figure 17. The amplitude of the harmonic disturbing forces depends on the rotational speed and, therefore, the x-y-plot looks different for different rotational speeds.

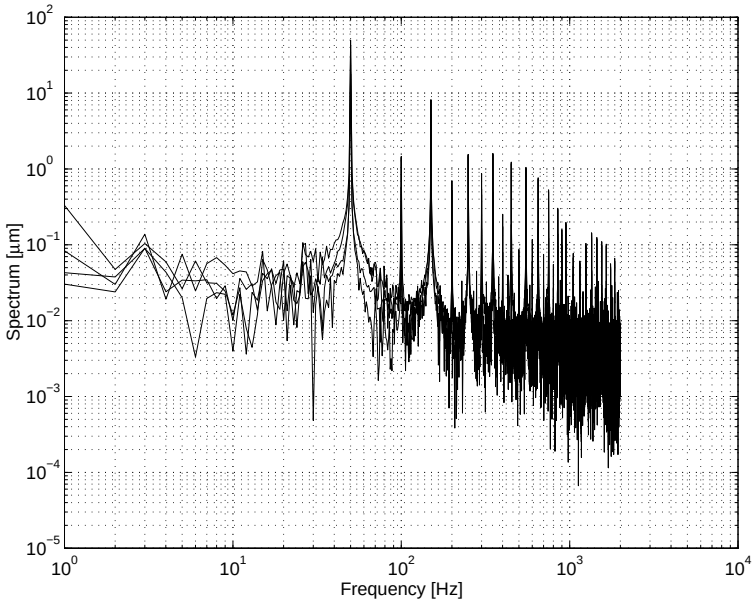

Figure 16: FFT of the time-domain signals from the four radial position sensors

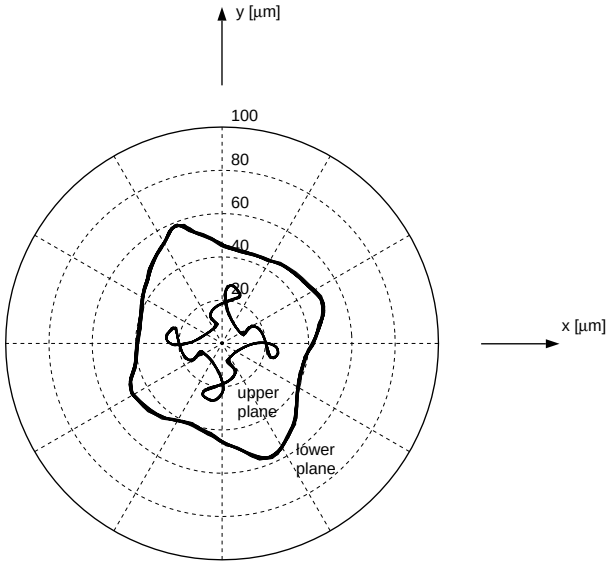

Figure 17: Measured x-y-plot of the rotor motion in the two radial bearing planes, rotational speed 3000 rpm, decentralized control (normal operation of the motor, voltage 280 V)

5 Conclusions and Outlook

A short time energy storage device with 1 kWh of usable energy and high power has been presented. The KIS system has strong gyroscopic coupling. Therefore, the rotor eigenfrequencies strongly depend on the rotational speed. Gyroscopic effects drastically decrease system performance and can cause instability when decentralized control or centralized control with LQR design is used. Cross feedback control is proposed. It leads to better system performance and avoids instability. Furthermore, it is easy to implement.

In a future step unbalance cancellation will be implemented. Housing vibrations have to be analyzed and filter design has to be optimized. Further measurements of loading/unloading behaviour, long-time and efficiency tests will be done. Meanwhile another project has been started in order to test a short time energy storage device for seam-welding machines in industry.

Acknowledgements

The project was funded by NEFF (Nationaler Energie Forschungs-Fond).
Project partners are the Institute of Electrical Machines and the Chair of Power Electronics and Electrometrology.

References

[AK95] M. Ahrens and L. Kučera. Cross Feedback Control of a Magnetic Bearing System. In *3rd International Symposium on Magnetic Suspension Technology*, Tallahassee, 1995.

[ATvBS94] M. Ahrens, A. Traxler, P. von Burg, and G. Schweitzer. Design of a Magnetically Suspended Flywheel Energy Storage Device. In *4th International Symposium on Magnetic Bearings*, Zurich, 1994.

[Ble84] H. Bleuler. *Decentralized Control of Magnetic Rotor Bearing Systems.* PhD thesis, ETH Swiss Federal Institute of Technology, Zurich, 1984.

[HBGL96] R. Herzog, P. Bühler, C. Gähler, and R. Larsonneur. Unbalance Compensation Using Generalized Notch Filters in the Multivariable Feedback of Magnetic Bearings. *IEEE Transactions on Control Systems and Technology, Special Issue on Magnetic Bearing Systems*, 1996.

[Her91] R. Herzog. *Ein Beitrag zur Regelung von magnetgelagerten Systemen mittels positiv reeller Funktionen und $\mathcal{H}^\infty$-Optimierung.* PhD thesis, ETH Eidgenössische Technische Hochschule, Zürich, 1991.

[LH94] R. Larsonneur and R. Herzog. Feedforward Compensation of Unbalance: New Results and Application Experiences. In *IUTAM Symposium The Active Control of Vibration*, Bath, 1994.

[Mag71] K. Magnus. *Kreisel, Theorie und Anwendungen.* Springer-Verlag, Berlin, 1971.

[ME93] A.M. Mohamed and F.P. Emad. Nonlinear Oscillations in Magnetic Bearing Systems. *Transactions on Automatic Control*, 38, August 1993.

[MH84] T. Mizuno and T. Higuchi. Design of the Control System of Totally Active Magnetic Bearings. In *International Symposium on Design and Synthesis*, Tokyo, 1984.

[MS76] P.C. Müller and W. Schiehlen. *Lineare Schwingungen.* Akademische Verlagsgesellschaft, Wiesbaden, 1976.

[ONS89] Y. Okada, B. Nagai, and T. Shimane. Cross Feedback Stabilization of the Digitally Controlled Magnetic Bearing. In *Conference on Mechanical Vibration and Noise*, Montreal, 1989. ASME.

[SG93] H. Stemmler and P. Guggenbach. Configuration of High-Power Voltage Source Inverter Drives. In *EPE 93*, Brighton, 1993.

[TUH95] R. Takahata, H. Ueyama, and H. Higasa. Basic Design of 1kWh Class Energy Storage Flywheel Rotor Using Superconducting Magnetic Bearings. In *1995 International Workshop on Superconductivity*, Maui, 1995.

[Ulb79] H. Ulbrich. *Entwurf und Lagerung einer berührungsfreien Magnetlagerung für ein Rotorsystem.* PhD thesis, TU München, 1979.

[vB95] P. von Burg. Stress Calculation Model for Thick Rim Flywheel. In *Enercomp 95*, Montreal, 1995.